THE JOURNAL OF PHYSICAL CHEMISTRY A
A JOURNAL OF THE AMERICAN CHEMICAL SOCIETY

pubs.acs.org/JPCA Article

σ-Donation and π-Backdonation Effects in Dative Bonds of Main-Group Elements

Brett A. Smith and Konstantinos D. Vogiatzis*

Cite This: J. Phys. Chem. A 2021, 125, 7956–7966 Read Online

ACCESS | Metrics & More | Article Recommendations | Supporting Information

ABSTRACT: The nature of donor–acceptor interactions is important for the understanding of dative bonding and can provide vital insights into many chemical processes. Here, we have performed a computational study to elucidate substantial differences between different types of dative interactions. For this purpose, a data set of 20 molecular complexes stabilized by dative bonds was developed (DAT20). A benchmark study that considers many popular density functionals with respect to accurate quantum chemical interaction energies and geometries revealed two different trends between the complexes of DAT20. This behavior was further explored by means of frontier molecular orbitals, extended-transition-state natural orbitals for chemical valence (ETS-NOCV), and natural energy decomposition analysis (NEDA). These methods revealed the extent of the forward and backdonation between the donor and acceptor molecules and how they influence the total interaction energies and molecular geometries. A new classification of dative bonds is suggested.

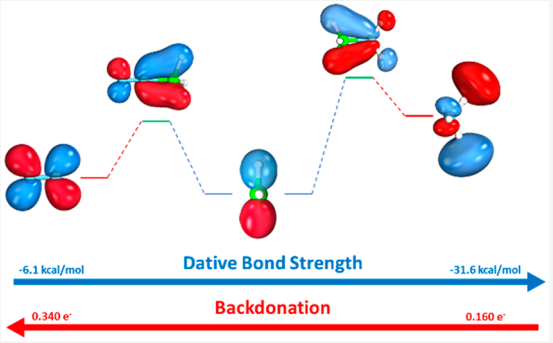

1. INTRODUCTION

The premise of dative bonds was first mentioned by Lewis' electron pair bonding model in the *Valence and the Structure of Atoms and Molecules*.[1] In this work, acids and bases were defined in terms of lone-pair electron acceptors and donors, respectively.[2] Lewis acid–base pairs that are formed through electron pair donation proceed through dative bonding, which presents an atypical bonding scheme and is reflected in their energies and geometric properties. Pauling described dative bonds as a "double bond" with one ionic and one covalent component, which has been referred to as a semipolar bond.[3] A key difference between a dative bond and a traditional covalent bond is seen at the dissociation limit (highlighted in Scheme 1). In a coordinate covalent (dative) bond, a pair of bonding electrons is donated to the acceptor species and bond dissociation proceeds heterolytically. In a traditional covalent bond, a single-bonding electron is provided by both species and bond dissociation proceeds homolytically.

Scheme 1. Dissociation of a Traditional Covalent Bond and a Dative Bond

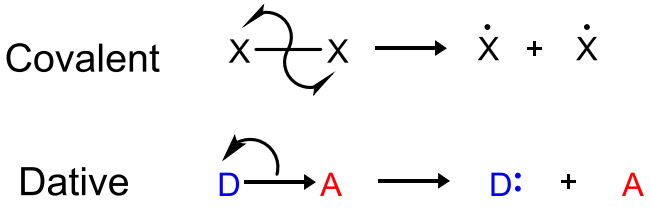

Currently, there are two prevailing metrics or descriptions of the degree of dative character in a bond. Weinhold and Landis have developed a qualitative criterion for dative bond characterization. The first states that dative bond formation is accompanied by a change in formal charge (Q) in both donor and acceptor, which should be equal in magnitude and with opposite sign[4]

$$Q_{\text{donor}} - Q^{0}_{\text{donor}} \cong -(Q_{\text{acceptor}} - Q^{0}_{\text{acceptor}}) \quad (1)$$

$$\Delta Q_{\text{donor}} \cong -(\Delta Q_{\text{acceptor}}) \quad (2)$$

where Q represents the atomic charge of a given species and the superscript "0" denotes the atomic charge of a given fragment. If ΔQ_{donor} is not equal to $\Delta Q_{\text{acceptor}}$, the difference in these changes is equal to the charge-transfer frustration $\Delta\Delta Q_{\text{D–A}}$ (D: donor, A: acceptor). This frustration manifests the compatibility of given donor and acceptor fragments.[5] This bonding scheme has been described as "atypical" because the mixing of ionic and covalent

Received: July 4, 2021
Revised: August 17, 2021
Published: September 3, 2021

https://doi.org/10.1021/acs.jpca.1c05956
J. Phys. Chem. A 2021, 125, 7956–7966

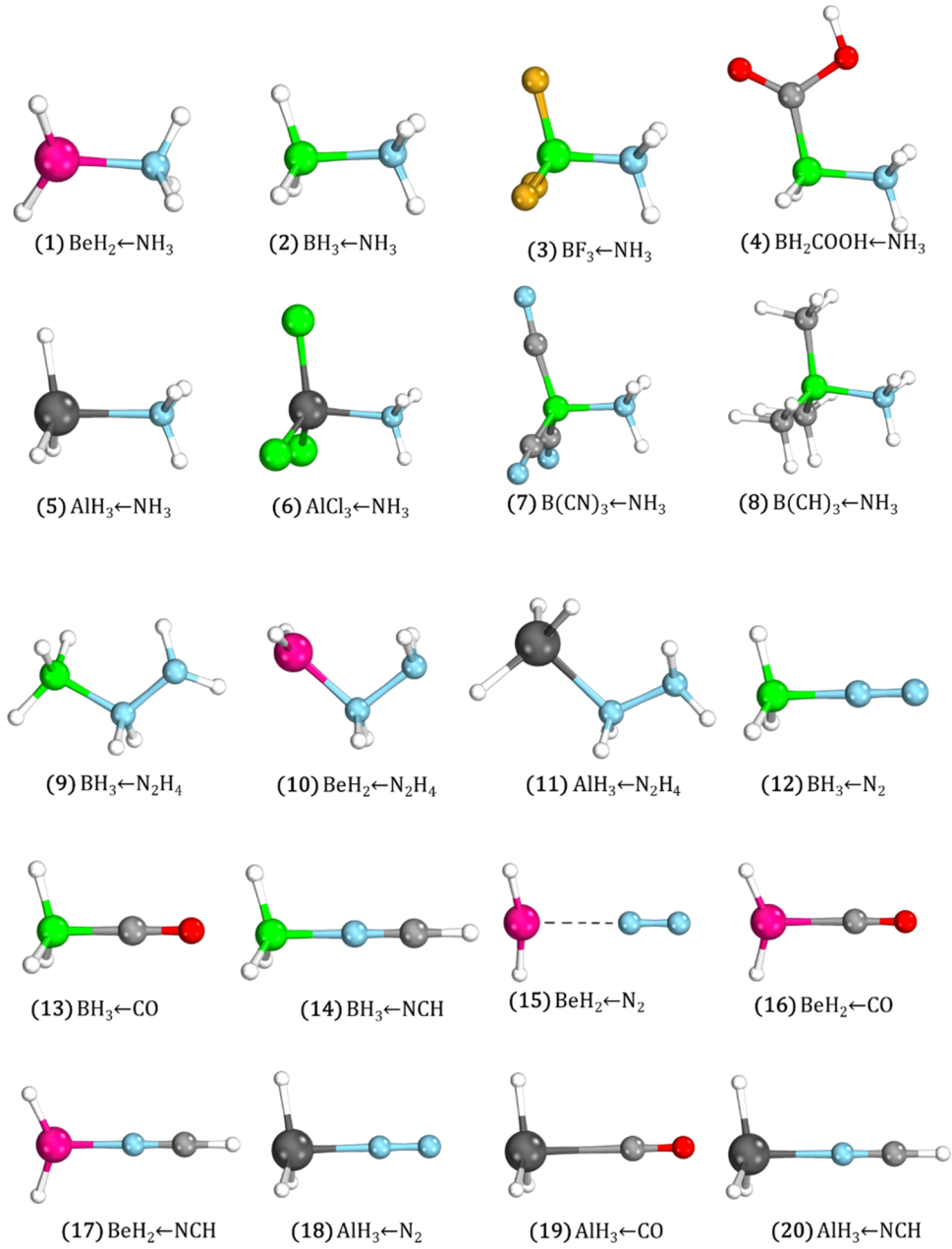

Figure 1. Twenty molecular complexes that form the DAT20 dative bond benchmark database. The DAT20 are split into type 1 and type 2 complexes. Complexes **1**−**11** belong to type 1 and complexes **12**−**20** belong to type 2.

character of the complex becomes more pronounced in comparison to purely covalent or ionic bonds.[5] Lepetit et al. have proposed a metric for a dative character that utilizes dative covalence energies that derive from the different homo- and heterolytic bond dissociation pathways.[6] Both charge-transfer frustration and dative covalence energies used as metrics for a dative character are extensions to Pearson's Hard−Soft Acid−Base[7] theory, where the strength of the bond is based upon the ionization energy of the donor and the electron affinity of the acceptor. Because of the inherent mixing of ionic and covalent potential energy surfaces,[8] the energies and molecular geometries of dative bonded molecular species have been the topic of quantum chemical studies,[9,10] which target to unravel the physics of main-group complexes and transition-metal complexes. The Dewar−Chatt−Duncanson model that is used frequently in transition-metal chemistry considers metal−ligand interactions in terms of forward donation from the ligand and backdonation from the metal. The nature of bonding in transition metals varies from main-group complexes in that d orbitals play a larger role in backdonation.[11] Complexes with dative bonds are prone to charge-transfer frustration and mixing of ionic and covalent potential energy surfaces. These phenomena can introduce artifacts in the computational modeling of structures containing dative bonds.

Density functional theory (DFT) is extensively used in computational studies due to its efficiency and relative accuracy. The accuracy of DFT is dependent on the choice of the density functional and its underlying approximations. Pure local-density approximations (LDA) and generalized gradient approximation (GGA) density functionals are known to overestimate the interaction energy of dative bonds,[12,13] whereas meta-GGA and hybrid functionals typically do not quantitatively capture mid-

https://doi.org/10.1021/acs.jpca.1c05956
J. Phys. Chem. A 2021, 125, 7956−7966

and long-range interactions.[14] Incorporating an appropriate amount of Hartree−Fock (HF) exchange can suppress the overestimated binding energy, but this is a nonsystematic, empirical observation that typically relies on error cancellation. The range-separated functionals properly model the asymptotic behavior of the exchange potential ($-r_{12}^{-1}$).[15,16] This is achieved through the partitioning of the Coulomb operator into a short- and long-range terms, which are smoothly connected by a range-separation parameter (μ). The ability to smoothly model the exchange potential at short and long ranges implements the correct physics of charge transfer and electron donation that are inherent in dative bonds, and thus, range-separated hybrid functionals can accurately capture dative interactions. On the contrary, post-HF wave-function theory-based methods do not rely on a functional choice, and their accuracy is systematically increased based on one-electron basis and the level of electron excitations (N-electron basis).[17]

Here, we present a novel classification of dative bonds based on the underlying interaction effects, including forward and backdonation. For that purpose, we developed DAT20, a balanced database composed by 20 molecular complexes formed by dative bonds (Section 2). The computational details of this study are presented in Section 3. Accurate interaction energies computed at the coupled-cluster singles-and-doubles with perturbative triples (CCSD(T)) at the complete basis-set limit (CBS) are used as reference.[18,19] The applicability of popular density functionals and the domain localized pair natural orbital CCSD(T) (DLPNO-CCSD(T)) is evaluated with respect to the reference data (Section 4).[20] The different types of donor−acceptor bonds led us to propose a classification between two different types of dative bonds, which was supported by a variety of computational methodologies based on frontier molecular orbitals, extended-transition-state natural orbitals for chemical valence (ETS-NOCV)[21] calculations, and natural energy decomposition analysis (NEDA).[22,23] The conclusions of this study are presented in Section 5.

2. DAT20 DATA SET

For the purposes of this study, the DAT20 data set was compiled, which is composed of 20 small main-group donor−acceptor pairs connected via dative bonds (Figure 1). Previous databases focused mainly on substituted amine boranes.[9,10] To the best of our knowledge, this is the first database of dative bonded systems that balances diversity in both composition and relative difficulty for computations (vide infra).

The DAT20 is split into two subsets. The first (type 1) includes complexes in a pseudostaggered configuration, which are composed of trigonal pyramidal acceptor fragments (AX_3) bonded to nitrogen-containing trigonal pyramidal donor fragments (complexes **1**−**11**). The first eight include ammonia as the electron donor: H_2Be-NH_3 (**1**),[24] H_3B-NH_3 (**2**),[1,8,25,26] F_3B-NH_3 (**3**),[27,28] H_2(COOH)B-NH_3 (**4**),[29] H_3Al-NH_3 (**5**), Cl_3Al-NH_3 (**6**), $(CN)_3$B-NH_3 (**7**),[9] and $(CH_3)_3$B-NH_3 (**8**).[1,8] Complexes **2**−**8** fit into the archetypical dative bond of amine boranes but still offer diversity in the acceptor molecule. In particular, complexes **5** and **6** are based on complexes **2** and **3**, respectively, but the borane is substituted by the alumane (AlH_3, aluminum hydride) acceptor molecule. The remaining three complexes of the type 1 subgroup include hydrazine as a donor molecule: H_2Be-$NH_2(NH_2)$ (**9**), H_3B-$NH_2(NH_2)$ (**10**), and H_3Al-$NH_2(NH_2)$ (**11**).

Type 2 complexes are characterized by a C_{2V} or C_{3V} molecular symmetry and include a linear donor fragment with sp-hybridized donor atoms (complexes **12**−**20**). Those are H_3B-N_2 (**12**),[30,31] H_3B-CO (**13**),[8,25,27,28] H_3B-NCH (**14**),[32] H_2Be-N_2 (**15**), H_2Be-CO (**16**), H_2Be-NCH (**17**), H_3Al-N_2 (**18**), H_3Al-CO (**19**), and H_3Al-NCH (**20**). The type 2 subgroup includes BH_3 (**12**−**14**), BeH_2 (**15**−**17**), and AlH_3 (**18**−**20**) as electron-accepting molecules and N_2, CO, and NCH as electron-donating molecules.

Our aim was to form a data set that represents a multitude of donor−acceptor interactions. The differences between type 1 and type 2 complexes are primarily observed in the nature and geometries of electron-donating molecules. Type 1 complexes also feature a variety of different electron-accepting molecules that lead to various inductive and substituent effects on donor−acceptor interactions. A detailed analysis of this behavior is provided in the next sections.

3. COMPUTATIONAL METHODS

3.1. Density Functional Theory Calculations. Density functional theory (DFT) geometry optimizations were performed on 20 complexes of the DAT20 data set. In this work, 10 density functionals were evaluated based on interaction energies (E_{INT}) and bond lengths in comparison to highly accurate reference calculations obtained by coupled-cluster theory calculations (vide supra). The following functionals were used in conjunction with the resolution of identity (RI) approximation[33] and Grimme's D3 empirical dispersion[34] correction with the Becke−Johnson (BJ) damping function[34,35] as implemented in the TURBOMOLE 7.2.1[36] software package: PBE,[37] BP86,[38] TPSS,[39] PBE0,[40] TPSSh,[41] B3LYP,[42] M06-2X[43] (without D3-BJ), and B2PLYP.[44] Geometry optimizations were performed using def2-TZVP and def2-TZVPP basis sets,[45,46] the corresponding auxiliary basis set,[47] and the m4 grid.[48] The range-separated hybrid functionals, CAM-B3LYP[49] and ωB97x-D3,[50,51] were also evaluated, as they are implemented in the ORCA 4.2.1[52] software package. Equivalent electron basis sets (def2-TZVP and def2-TZVPP), auxiliary basis sets, approximations (RI and D3-(BJ)), and grid size were employed to ensure consistency (Lebdev's spherical 434-point grid). The interaction energies (E_{INT}) are calculated based on the energy difference between the electron donor (E_D^0) and electron acceptor (E_A^0) fragments in their relaxed geometries, while preparation energies for the donor (E_{prep}^D) and acceptor (E_{prep}^A) fragments were computed as

$$E_{INT} = E_{DA} - (E_D^0 + E_A^0) \quad (3)$$

$$E_{prep}^D = E_D^0 - E_D^{AD} \quad (4)$$

$$E_{prep}^A = E_A^0 - E_A^{AD} \quad (5)$$

where E_D^{AD} and E_A^{AD} are the energies of donor and acceptor fragments in the A−D supersystem geometry, respectively, and E_D^0 and E_A^0 are the energies of relaxed donor and acceptor molecules, respectively.

3.2. Explicitly Correlated Coupled-Cluster Calculations. For generating reference energies and geometries of 20 molecular systems (DAT20), the donor−acceptor bond distance was stretched in systematic increments, as shown in Tables S22−S27 in the Supporting Information. At each increment, a constrained geometry optimization was performed at the M06-2X/def2-TZVP level of theory for relaxing the position of all other atoms. Explicitly correlated CCSD calculations were then performed at each donor−acceptor

https://doi.org/10.1021/acs.jpca.1c05956
J. Phys. Chem. A 2021, 125, 7956−7966

bond length for the generation of potential energy curves. We have applied two different approaches for the estimation of the energy at the complete basis-set limit. First, explicitly correlated (F12) methods[53] were employed for CCSD, which include functions that depend on interelectronic coordinates to converge toward the CBS limit. The frozen core approximation together with the cc-pV*X*Z-F12[54,55] basis sets (X = T, Q) and the corresponding complementary auxiliary basis set (CABS) was used. The cc-pVXZ-F12 was also used for fitting F12 and electron-repulsion integrals (CBAS) and two-electron contributions to the Fock matrix (JKBAS). The 2B ansatz was used in all F12 calculations.[56] The two-point extrapolation scheme of Helgaker and co-workers was applied for estimating the CBS of the perturbative triples.[57] All reference energies $E_{CCSD(F12)(T)/CBS}$ used in this work were computed as

$$E_{CCSD(F12)(T)/CBS} = E_{HF/QZ} + \delta E_{CAB\,S/QZ} + \delta E_{CCSD(F12)/QZ} + \delta E_{(T)/CBS} \quad (6)$$

$$\delta E_{(T)/CBS} = \frac{\delta E_{(T)/XZ} X^3 - \delta E_{(T)/YZ} Y^3}{X^3 - Y^3} \quad (7)$$

where $E_{HF/QZ}$ is the HF energy and the δ symbol indicates electron correlation terms. CABS S is the CABS singles' correction term to the HF energy. TZ and QZ correspond to the cc-pVTZ-F12 and cc-pVQZ-F12 basis sets with cardinal numbers X = 3 and Y = 4, respectively. All CCSD(F12)(T) calculations were performed with the TURBOMOLE 7.2.1[36] quantum chemical program package.

3.3. Domain Localized Pair Natural Orbital Coupled-Cluster Calculations. Domain localized pair natural orbital coupled-cluster DLPNO-CCSD(T) computations were performed for all systems included in DAT20.[20] All DLPNO-CCSD(T) calculations were performed with the ORCA 4.2.1 program package using the TightPNO cutoff, the cc-pVQZ basis set, and cc-pVQZ/C complimentary auxiliary basis set. All calculations followed the same methodology shown in the CCSD(F12)(T) reference calculations.

3.4. ETS-NOCV Analysis. Extended-transition-state natural orbitals for chemical valence[21] (ETS-NOCV) calculations were performed with the ORCA 4.2.1[52] software package, the ωB97x-D3[51] functional, and the def2-TZVP[45,46] basis set. For the purposes of understanding the donor−acceptor interactions of DAT20, we considered NOCVs that had an eigenvalue of at least 0.05 e^-.

3.5. Natural Energy Decomposition Analysis. Natural energy decomposition analysis (NEDA) was performed as implemented with Gaussian 16 (Rev. C.)[58] and NBO 7.0.8.[59] This methodology decomposes the interaction energy into five components, electrostatic (ES), polarization (POL), charge transfer (CT), exchange (EX), and deformation (DEF). In recent implementations of the NEDA approach, these components are reduced into three components: electrical interactions (EL), charge transfer (CT), and repulsive interactions (CORE). The electrical interactions (ES) are composed of the electrostatic interaction, polarization, and the electrical self-energy. The repulsive interactions (CORE) are composed of the intermolecular exchange of like-spin electrons, the deformation energy, and the electrical self-energy.

$$\Delta E = ES + POL + CT + EX + DEF \quad (8)$$

$$EL = ES + POL + SE \quad (9)$$

$$CORE = EX + DEF - SE \quad (10)$$

$$\Delta E = EL + CT + CORE \quad (11)$$

NEDA calculations were performed for 20 complexes of the DAT20 data set with all functionals included in this study, except B2PLYP, since it is not yet interfaced with the decomposition analysis method. All functionals showed similar behavior, and thus, we have analyzed the results obtained from ωB97x-D3. For more details, we refer the reader to the Supporting Information, Section S7.

4. RESULTS AND DISCUSSION

4.1. Reference Data. Reference interaction energies and bond lengths between donor (D) and acceptor (A) molecules for the 20 complexes of DAT20 were obtained at the explicitly-correlated coupled-cluster singles-and-doubles with perturbative triples (CCSD(T)) at the complete basis-set limit or CCSD(F12)(T)/CBS level of theory (Table 1). The CBS limit is computed by explicitly correlated (F12) methods and basis-set extrapolation schemes. The type 1 subgroup (complexes **1**−**11**) exhibits stronger interaction energies (average E_{INT} = −31.52 kcal/mol) and shorter bond lengths (average R_{D-A} = 1.78 Å). On the contrary, type 2 (complexes **12**−**20**) exhibits weaker interaction energies (average E_{INT} = −11.81 kcal/mol) and longer donor−acceptor bond lengths (average R_{D-A} = 1.96 Å). $(CN)_3B\text{-}NH_3$ (**7**) exhibits the strongest donor−acceptor interaction among the data set (E_{INT} = −48.19 kcal/mol), and it has the shortest donor−acceptor bond length (R_{D-A} = 1.62 Å) among the type 1 complexes. The type 2 complex $H_3B\text{-}CO$ (**13**) not only exhibits the shortest donor−acceptor bond length (1.54 Å) but also has an interaction energy that is below the average of the type 1 complexes (E_{INT} = −25.41 kcal/mol).

A systematic increase in the interaction strength within the type 2 complexes was found based on the donor species. This

Table 1. Donor−Acceptor Bond Lengths (Å), Interaction Energies (E_{INT}), and Preparation Energy of Donor (E^D_{prep}) and Acceptor (E^A_{prep}) Species for Complexes 1−20 Calculated at the CCSD(F12)(T)/CBS Level of Theory[a]

complex	bond length	E^A_{prep}	E^D_{prep}	E_{INT}
1	1.77	−8.67	−0.14	−25.29
2	1.64	−13.03	−0.08	−31.64
3	1.68	−35.27	−0.17	−22.74
4	1.63	−18.58	−0.16	−38.78
5	2.13	−3.39	−0.09	−29.71
6	1.99	−16.33	−0.14	−39.92
7	1.62	−18.10	−0.22	−48.19
8	1.68	−2.38	−0.14	−18.09
9	1.64	−12.53	−1.66	−35.83
10	1.75	−8.21	−4.70	−25.33
11	2.05	−3.62	−1.61	−31.21
12	1.64	−7.68	−1.19	−6.10
13	1.54	−11.68	0.05	−25.35
14	1.59	−11.58	−0.31	−20.52
15	2.45	−0.85	−1.24	−0.92
16	1.92	−5.29	2.67	−5.28
17	1.76	−7.58	−0.28	−12.99
18	2.31	−1.79	−1.22	−5.99
19	2.36	−0.75	−0.20	−10.76
20	2.06	−2.81	−0.29	−18.36

[a]All energy values are given in kcal/mol.

https://doi.org/10.1021/acs.jpca.1c05956
J. Phys. Chem. A 2021, 125, 7956−7966

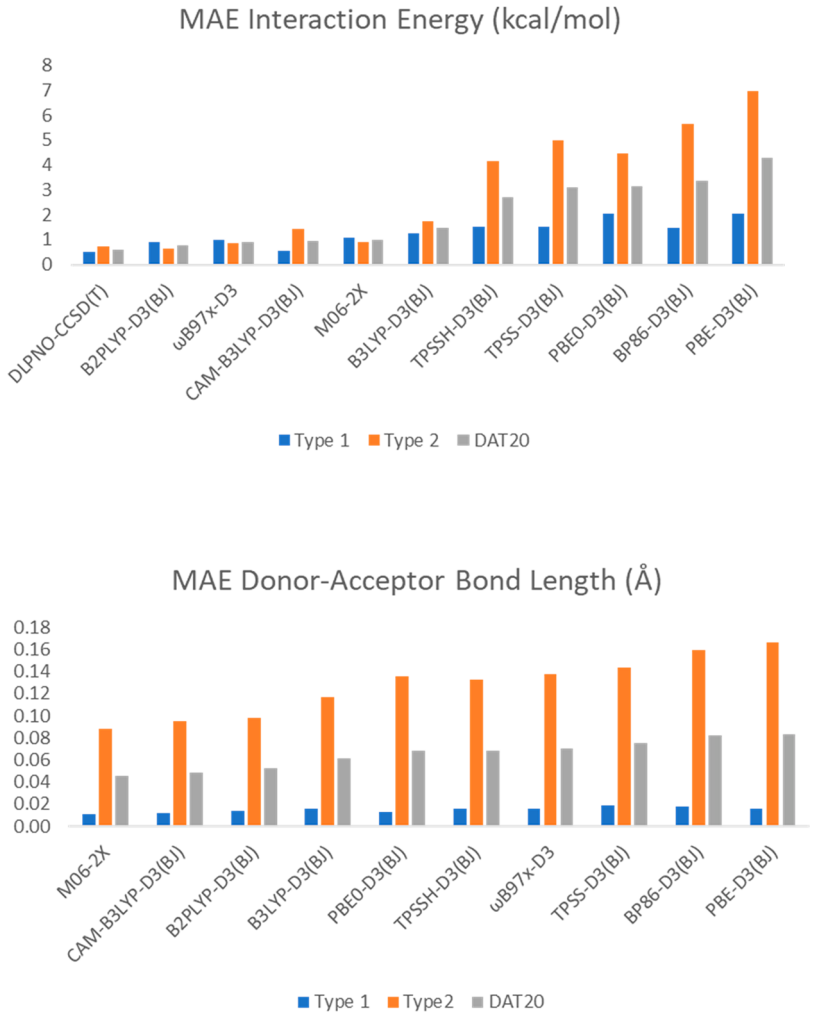

Figure 2. Mean absolute error (MAE) in the interaction energy (left) and the donor−acceptor bond length (right). The bars have been separated to show the MAE of each method in terms of the type 1 complexes (blue), type 2 complexes (orange), and the total DAT20 (gray).

trend follows the N_2 < CO < NCH order. For example, for the three cases that BH_3 was considered as an acceptor (**12**−**14**), the computed interaction energies were −6.10, −20.52, and −25.35 kcal/mol. The uncharacteristically short but weak bond of complex **12** arises from dinitrogen's lone pair, as discussed in a previous study.[30] Complex **13** exhibits the shortest donor−acceptor bond length in the data set, which is largely due to the terminal oxygen's ability to accept electrons in the backdonation process. Complex **14**[32] is part of nitrile boranes that have been studied extensively and are known to bind strongly to boranes.[30] This donor−acceptor pair exhibits the strongest binding energy of the type 2 interactions due to the increased lone-pair donation. The analysis provided in the following sections further explains the bonding behavior of complexes **13** and **14**.

It is also important to discuss the differences between the various acceptor types. Complexes that contain beryllium hydride (**1**, **10**, **15**−**17**) slightly deviate from their type 1 and 2 counterparts. In the type 1 beryllium hydride-based complexes (**1**, **10**), interaction energies are lower than the interaction energies of their borane- and alumane-based counterparts. In the most basic complexes, i.e., those that utilize an ammonia donor, the interaction energy for BeH_2 is −25.29 kcal/mol, whereas the borane- and alumane-based complexes have interaction energies of −31.65 and −29.71 kcal/mol, respectively. This behavior can be explained in terms of the electron affinity of the central atom in the acceptor molecule; beryllium has the lowest electron affinity (in magnitude), making it a less suitable acceptor species. The R_{D-A} bond lengths show the same trend, where complex **1** shows an increased bond length of 1.77 Å compared to complex **2** (R_{D-A} = 1.65 Å). Additionally, the H−Be−H bond angle in Be-containing complexes correlates well with the strength of the interaction. The type 2 complexes **15**−**17** exhibit H−Be−H bond angles of 166.7, 147.3, and 141.1°, respectively, and interaction energies of −0.92, −5.28, and −12.99 kcal/mol, respectively (see the Supporting Information, Table S4). Similarly, the type 1 complexes **1** and **10** exhibit H−Be−H bond angles of 138.7 and 139.8° (ΔE_{INT} = −25.29 and −25.33 kcal/mol), respectively, which further justifies that deviation from the H−Be−H linearity leads to strong interaction energies since the presence of a donor molecule will affect the electronic structure and geometry of the acceptor molecule.

To further understand the nature of the donor−acceptor interactions present in DAT20, we have calculated and analyzed the energy associated with the geometric changes between an isolated fragment and its conformation in the donor−acceptor supersystem geometry (preparation energy or deformation energy), which is a good measure of electronic and geometric changes necessary to form the complex. In addition, the important geometric changes in isolated fragments during dative bond formation reflect the strength and nature of the

https://doi.org/10.1021/acs.jpca.1c05956
J. Phys. Chem. A 2021, 125, 7956−7966

interaction. For example, the isolated borane, substituted borane, and aluminum hydride undergo a change in hybridization from sp^2 to sp^3 upon bond formation, which is reflected in the deviation from planarity. Beryllium hydride differs from the aforementioned cases, as the change in hybridization occurring is sp to sp^2. The geometric changes in the H−Be−H bond angle are larger than the other acceptor cases, but these changes require less energy as there is less steric repulsion between beryllium's hydrogen substituents. A detailed account of geometric parameters and preparation are provided in Section S3 of the Supporting Information.

4.2. Benchmarking of Density Functionals for Dative Bonds. The 20 molecular structures of DAT20 were used for the evaluation of the performance of 10 popular density functionals. Their accuracy was tested based upon two metrics: the binding energy and the donor−acceptor distances. To evaluate the performance of each density functional, the mean absolute error (MAE) was calculated with respect to CCSD(F12)(T)/CBS energies at the complete basis-set limit. In addition, the correlated DLPNO-CCSD(T) method is compared to the reference data, as it is a computationally more affordable alternative to the more complete CCSD(F12)(T)/CBS level. All results are reported in Section S4 of the Supporting Information.

The MAE for both binding energy (kcal/mol) and donor−acceptor bond length (Å) are given in Figure 2. The GGA functionals PBE-D3(BJ) and BP86-D3(BJ) showed the lowest accuracy among the functionals considered in this study, with a MAE of 4.28 and 3.36 kcal/mol, respectively. TPSS-D3(BJ) and PBE0-D3(BJ) provided more accurate interaction energies (3.13 and 3.09 kcal/mol, respectively), while TPSSh-D3(BJ) showed a MAE of 2.70 kcal/mol. Major improvements were introduced by B3LYP-D3(BJ), which showed a MAE of 1.47 kcal/mol. This study identified four density functionals as top performers with MAE less or close to 1.00 kcal/mol. The double-hybrid B2PLYP-D3(BJ) is the most accurate (0.80 kcal/mol), followed by ωB97x-D3, CAM-B3LYP-D3(BJ), and M06-2X with MAEs in interaction energies of 0.93, 0.94, and 1.01 kcal/mol, respectively. Finally, the correlated DLPNO-CCSD(T) method provided reliable interaction energies below 1 kcal/mol (MAE of 0.62 kcal/mol). Thus, based on the analysis performed on the DAT20 database, DLPNO-CCSD(T) can be used as a reference method on larger molecular systems where conventional CCSD(T) calculations will be prohibitively costly.

The MAE of the donor−acceptor bond lengths computed by all methods considered in this study are shown in Figure 2 (right). The accuracy of these methods on the interatomic distance follows the same order as for the interaction energies. The only minor difference is observed for M06-2X and ωB97x-D3, where their order has been reversed, as ωB97x-D3 provided less accurate bond distances on average and was subject to an uncharacteristic large error in the nonbonding case of H_2Be-N_2 (**15**). It is also evident that the MAE in the donor−acceptor bond length is relatively low in type 1 complexes but is significantly higher in type 2 complexes, in line with interaction energy deviations.

The organization of DAT20 complexes into type 1 and type 2 revealed an interesting trend for almost all density functionals considered in this study. All functionals showed an increased error for type 2 complexes, except B2PLYP-D3(BJ), M06-2X, CAM-B3LYP-D3(BJ), and ωB97x-D3, which demonstrated similar deviations for both subgroups. For example, the MAE of PBE-D3(BJ) is 2.06 kcal/mol for type 1 complexes, but it has an increased MAE of 6.99 kcal/mol for type 2, an error that originates from the lack of nonlocal Hartree−Fock exchange (see the Supporting Information, Section S5). In the following subsections, the origin of the deviations between type 1 and type 2 complexes is further analyzed.

4.3. Forward and Backdonation Based on Frontier Molecular Orbitals. A primary characteristic of dative bonds is the interplay between forward donation and backdonation (Figure 3). The energy associated to the forward donation is

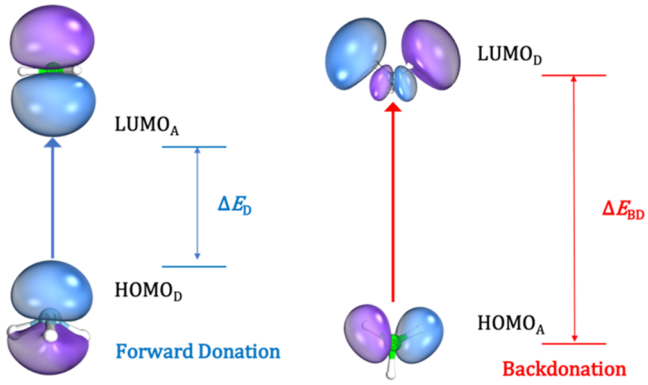

Figure 3. Representation of the orbitals involved in the lone-pair donation (left) and subsequent backdonation (right) characteristic of dative bonds.

correlated with the difference in energy of the donor's highest occupied molecular orbital (HOMO; $HOMO_D$ or H_D) and the acceptor's lowest unoccupied molecular orbital (LUMO; $LUMO_A$ or L_A). We will refer to this orbital energy difference as ΔE_D. Backdonation originates from the interaction between acceptor's HOMO ($HOMO_A$ or H_A), which has a predominant p_x or p_y character, and the donor's LUMO ($LUMO_D$ or L_D). Thus, the energy associated with backdonation can be described by the difference in energy of the acceptor's highest occupied orbitals and the donor's lowest unoccupied orbitals (ΔE_{BD}).

Figure 4 features the energy of the orbitals involved in donation and backdonation (in E_h), and their corresponding energy differences ΔE_D and ΔE_{BD} (in E_h). The red and blue color code corresponds to forward and backdonation, respectively, as shown in Figure 3. Small ΔE_D, i.e., strong forward donation, combined with weak backdonation (large ΔE_{BD}) leads to stronger binding energies, as demonstrated for complexes **4**, **6**, and **7** (ΔE_{INT} = −38.78, −39.42, and −48.19 kcal/mol, respectively).

An additional metric that we introduce in this study is the $\Delta\Delta E_{D-BD}$ defined as the difference between the forward (ΔE_D) and backdonation (ΔE_{BD}), which is shown in Figure 4. The physical meaning of the $\Delta\Delta E_{D-BD}$ value can be considered as the magnitude of the competing forward and backdonation mechanisms. The importance of this metric becomes more evident upon a comparison of the type 1 and type 2 complexes. All type 1 complexes have negative $\Delta\Delta E_{D-BD}$ values (Figure 4, top) that range between −0.152 eV (**8**) and −0.643 eV (**7**). However, there is no evident correlation between $\Delta\Delta E_{D-BD}$ and interaction energies since the exact extent of the forward and backdonation is hindered. On the contrary, the $\Delta\Delta E_{D-BD}$ value becomes important for the type 2 complexes. As seen at the bottom of Figure 4, the $\Delta\Delta E_{D-BD}$ value is either positive or slightly negative (−0.018 and −0.044 eV for **13** and **14**, respectively). Additionally, the two systems with negative

https://doi.org/10.1021/acs.jpca.1c05956
J. Phys. Chem. A 2021, 125, 7956−7966

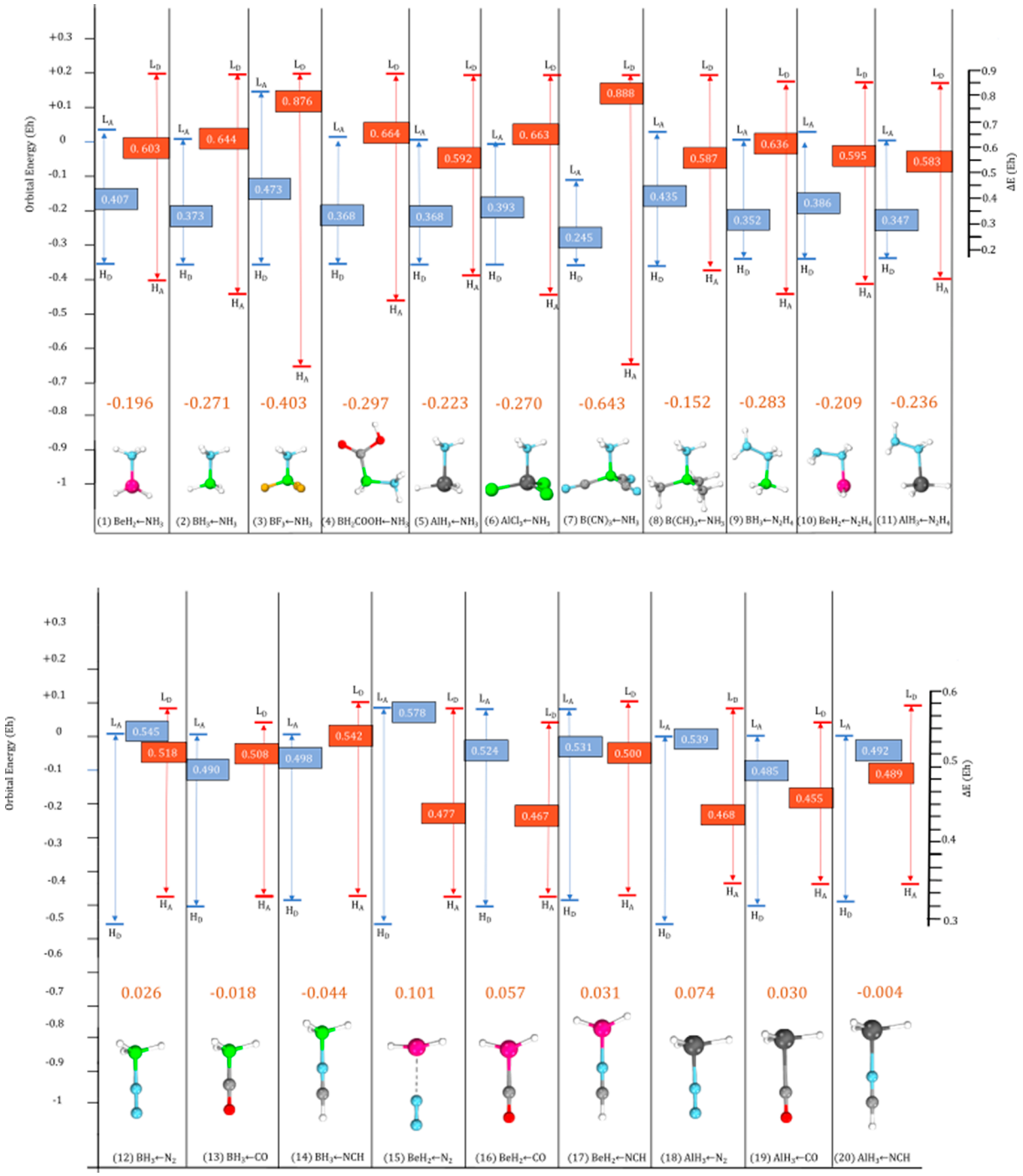

Figure 4. HOMO−LUMO gaps (in E_h) of type 1 (top) and type 2 (bottom) complexes computed at the ωB97x-D3/def2-TZVP level (blue: electron donation, red: backdonation). The $\Delta\Delta E_{D-BD}$ energy metric for each molecular complex is shown in orange font.

$\Delta\Delta E_{D-BD}$ have the strongest interaction among the type 2 complexes with ΔE_{INT} of −25.35 and −20.52 kcal/mol, respectively.

In addition to the DAT20, 270 complexes containing dative bonds were introduced to the study to validate the use of the ΔE_D, ΔE_{BD}, and $\Delta\Delta E_{D-BD}$ metrics as a means of characterizing a dative bond. These 270 complexes were modeled according to Scheme S1, using Molsimplify's structure generation capabilities.[60,61] Geometry optimizations were performed for each molecular system and their respective relaxed fragments at the ωB97x-D3/def2-TZVP level of theory followed by the same orbital analysis as described in this subsection. The differing behavior of type 1 and type 2 interactions is highlighted in Figure 5. Comparison of the ΔE_D values shows that type 2 interactions experience less accessible σ-donation (higher ΔE_D) than the type 1 interactions. The average ΔE_D for type 1 complexes is 0.39 E_h, whereas the average for type 2 is 0.52 E_h. The differences between the two interactions become even clear when comparing the values for $\Delta\Delta E_{D-BD}$, as the average type 1 interaction is −0.15 E_h, and the average type 2 interaction is 0.026 E_h, in agreement with the results of DAT20. Figure 5 also depicts how this quantity relates to the interaction energy; type 1 interactions experience lower and negative $\Delta\Delta E_{D-BD}$ values and stronger interactions. Type 2 interactions experience higher and

https://doi.org/10.1021/acs.jpca.1c05956
J. Phys. Chem. A 2021, 125, 7956−7966

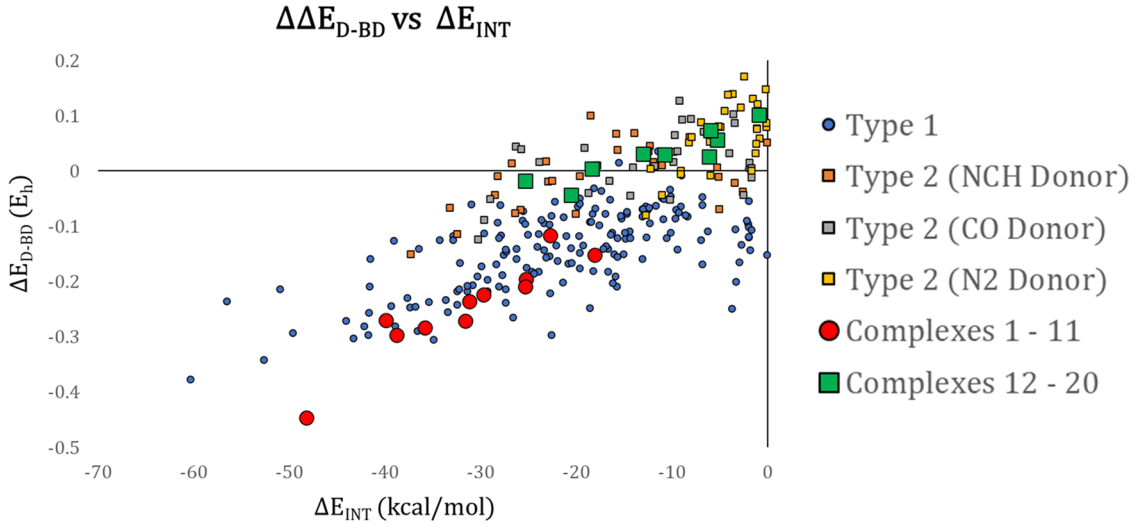

Figure 5. Scatter plot of the interaction energy ΔE_{INT}, and the difference in energy of the lone-pair donation and subsequent backdonation, $\Delta\Delta E_{D-BD}$. The circular points are associated with a type 1 interaction, where the original eleven type 1 complexes of DAT20 are shown in red color, and the 180 additional complexes are shown in blue color. The square points are associated with type 2 interactions, where the original nine type 2 complexes of DAT20 are shown in green color, and the 90 additional complexes are whoen in orange (NCH as donor), gray (CO as donor) and yellow (N_2 as donor).

positive $\Delta\Delta E_{D-BD}$ values and weaker interactions. This metric provides a physical insight into the differing interactions. Type 1 complexes lower the energy of lone-pair donation and destabilize the energy for backdonation, leading to greater net electron donation from donor to acceptor. Type 2 complexes raise the energy of the lone-pair donation and lower that of the backdonation; this hinders the net electron donation from donor to acceptor because there is a competitive nature to the forward and backdonation.

The fact that all type 2 complexes have $\Delta\Delta E_{D-BD}$ values closer to 0 than the type 1 molecular systems originates from the competitive forward and backdonation processes. Thus, the $\Delta\Delta E_{D-BD}$ metric can be considered as an effective descriptor between the two different types of dative bonds. Correlation was found between $\Delta\Delta E_{D-BD}$ and the interaction energy (Figure S3 of the Supporting Information); this evidence supports the difference in type 1 and type 2 dative interactions.

4.4. ETS-NOCV Analysis. In addition to the analysis based on canonical molecular orbitals described in the previous subsection, we have examined the DAT20 data set by means of ETS-NOCVs. Our aim is to provide a quantification of forward and backward electron donations and a qualitative description of the behavior of each donor−acceptor interaction. The results of ETS-NOCV calculations provide three descriptors of chemical relevance: (1) chemical valence eigenvalues (ν_k) that correspond to the number of electrons exchanged in a particular NOCV, (2) the orbital mixing between fragments (ΔE_{ORB}), and (3) qualitative natural orbitals for chemical valence that describe the donor−acceptor interaction. Additionally, ETS-NOCV analysis can partition the electron donation process into forward (ν_k^d) and backward donation (ν_k^{bd}). In a similar manner, the retention of donated electron density can be expressed as the difference between the chemical valence eigenvalues for donation and backward donation (ν_k^{d-bd}).

Each molecular system in DAT20 (excluding $H_2Be\text{-}N_2$) has four NOCVs that contributed to bonding (see the Supporting Information, Section S8). Our results indicate differences in electron donation and backdonation between type 1 and type 2 complexes. In type 1 complexes, the magnitude and retention of the lone-pair donation (average ν_k^d = 0.442 e^-) is greater than that of the subsequent backdonation process (average ν_k^{bd} = 0.321 e^-), which is in agreement with the previous molecular orbital analysis. Both NH_3 and N_2H_4 acceptor molecules stabilize lone-pair donation through their accessible HOMO orbitals and destabilize the backdonation process through their high-energy LUMO orbitals. The destabilization of the donor's LUMO orbitals leads to a greater retention of donated electron density and stronger interaction energies seen in type 1 complexes (average $\Delta\nu_k^{d-bd}$ = 0.121 e^-).

For the type 1 complex with the strongest dative bond (**7**, $(NC)_3B\text{-}NH_3$), the increased binding energy can be attributed to the low-lying LUMO and the strong donation and lack of backdonation (Supporting Information, Table S17). In most type 1 cases, the central acceptor atom (A = Be, B, or Al) accepts electrons from the donor (D), and releases electron density to its neighboring atoms (R) in the backdonation process (D: → A → R). However, for $(NC)_3B\text{-}NH_3$ (**7**), the lone-pair donation is directed toward the central boron (ν_k^d = 0.662 e^-), and the terminal nitrogen atoms accept electron density from their neighboring carbon, rather than pulling electron density from the central boron (D: → B−C → N). This allows for boron and ammonia to be more electronically saturated, leading to less backdonation from acceptor to donor (ν_k^{bd} = 0.396 e^-). Qualitatively, NOCVs of this complex exhibit highly covalent behavior, where almost no electron density is donated by the central boron atom.

Type 2 complexes display a more complex behavior, favoring the backdonation process (average ν_k^{bd} = 0.462 e^-) over the lone-pair donation (average ν_k^d = 0.323 e^-). The lone-pair donation process flows outward from the sp-hybridized donor (R ← D: → A) toward the neighboring atoms (R) and the acceptor (A). The now electron-deficient donor species attract electrons from both sides in the subsequent backdonation process (R → D: ← A). The case of $H_3B\text{-}CO$ (**13**) differs slightly since carbon acts as a conduit for oxygen in lone-pair donation (O → C → BH_3) and in the backdonation process allowing oxygen to accept electrons from borane through carbon (O ← C ← BH_3). This makes carbon monoxide not only a very good lone-pair donor (ν_k^d =

https://doi.org/10.1021/acs.jpca.1c05956
J. Phys. Chem. A 2021, 125, 7956−7966

0.593 e^-) but also increases the backdonation (ν_k^{bd} = 0.870 e^-), which is the origin of weaker interaction energies and contracted bond length. In complex **14**, the lone-pair donation is strong (ν_k^{d} = 0.480 e^-) and the backdonation process is destabilized and weaker than the other type 2 complexes (ν_k^{bd} = 0.652 e^-). Additionally, the orbital stabilization associated with orbital mixing is significantly higher than other complexes and is the highest in the entire data set (ΔE_{ORB} = −104.52 kcal/mol). Thus, the presence of both strong overlap and destabilized backdonation explains the strength of the dative bond in complex **14**.

4.5. Natural Energy Decomposition Analysis (NEDA). Natural energy decomposition analysis (NEDA) was performed to elucidate the effects and importance of charge transfer (CT), electrical interaction (EL, the classical-like Coulombic interactions), and core repulsion on the dative bond behavior. Dative bonds exhibit a net repulsive electrostatic interaction, given by the difference in the electrical interaction and core repulsions (EL-CORE). The sum of the core repulsion and electrical interaction indicates whether there is a favorable electrostatic interaction (negative value) or an unfavorable repulsive interaction (positive value). Due to net repulsion, charge-transfer interactions are the dominating stabilizing force in dative bonds, as this is synonymous with electron donation.

The ratio of charge transfer to electrostatic interaction shows the ability to distinguish between type 1 and type 2 complexes. Type 1 complexes show a stronger charge-transfer interaction to electrostatics, whereas type 2 complexes show a decreased charge transfer to electrostatics ratio (Supporting Information, Figure S5). Linear regression was performed to predict charge transfer and electrostatic interactions, and complexes above this prediction favor weak dispersion and induction stabilization (weak charge transfer), and complexes below this line favor stronger charge-transfer interactions. Interestingly, most type 1 complexes (**1**−**7**, **9**−**11**) are shown below the diagonal line, favoring strong charge-transfer interactions. The only type 1 complex above the prediction is complex **8** (Me_3B-NH_3), where methyl groups favor the weak induction interactions, but partially retain the donor−acceptor behavior of other type 1 complexes. On the contrary, type 2 complexes (**12**−**20**) are shown above the diagonal, weakening the charge transfer and favoring weaker dispersion and induction interactions. These observations are congruent with the results of both the frontier molecular orbital analysis and ETS-NOCV calculations.

5. CONCLUSIONS

Dative bonding presents an atypical bonding scheme with complex interactions, which is reflected in the bond strength and length. Here, an in-depth computational analysis of a data set of 20 complexes that contain dative bonds (DAT20) composed by main-group elements was discussed. DAT20 contains complexes with diverse interactions ranging from strong dative bonds (about −50 kcal/mol) to weak dative bonds (−1 to −5 kcal/mol). Additionally, DAT20 has exemplified the inconsistent nature of the bond length and interaction strength tradeoff between type 1 and type 2 complexes, as discussed for borane-containing complexes. Complex **2** (BH_3-NH_3) and its type 2 counterparts (**12**−**14**) have comparable donor−acceptor atom distances but the interaction energy of **2** is constantly stronger than the other three cases.

As a first step, we obtained highly accurate interaction energies and geometries with explicitly correlated coupled-cluster theory. The CCSD(F12)(T)/CBS results were used for identifying density functionals that reliably describe geometries and interaction energies of molecular systems bound through dative bonds. In particular, double-hybrid, range-separated, and highly parameterized functional with high amounts of HF exchange (B2PLYP-D3(BJ), CAM-B3LYP, ωB97x-D3, and M06-2X) provided the highest accuracy with respect to the coupled-cluster reference. The initial benchmark study revealed that most density functionals showed large deviations for a subgroup of the DAT20 database. Based on these findings, we propose a classification of dative bonds between main-group complexes in two main categories. The first (type 1) includes dative bonds that exhibit the traditional amine−borane architecture, whereas type 2 dative bonds exhibit sp-hybridized donor fragments (pseudo-C_{2V}). This study employed three complementary methodologies for describing the nature of interactions present in DAT20: frontier molecular orbital analysis, extended-transition-state natural orbitals for chemical valence (ETS-NOCV), and natural energy decomposition analysis (NEDA). Each of the three methods explained the nature of these interactions in a different manner. The frontier molecular orbital analysis provided a quantitative description of the orbital energies involved in lone-pair donation and subsequent backdonation that is characteristic of dative bonds. The results showed that the type 2 complexes stabilized the backdonation in terms of orbital energies. ETS-NOCV analysis provided both quantitative and qualitative descriptions of the lone-pair donation and backdonation processes. The results showed that the type 1 complexes stabilized lone-pair donation and destabilized the backdonation. Type 2 complexes showed small changes in lone-pair donation, instead strongly stabilizing the backdonation process. Finally, NEDA calculations provided a different perspective, showing that the type 1 complexes had less electrostatic repulsion than the type 2 complexes. The three methodologies were in agreement with respect to the role of backdonation as a destabilizing factor to the interactions present in the two subgroups of DAT20. In particular, the type 2 complexes showed an increased orbital overlap leading to larger backdonation, which increases the donor−acceptor repulsion and lowers the energy of the dative bond. We are currently exploring these two classes on molecular complexes that exhibit charge-transfer frustration, as well as on coordination bonds that involve transition metals.

■ ASSOCIATED CONTENT

Supporting Information

The Supporting Information is available free of charge at https://pubs.acs.org/doi/10.1021/acs.jpca.1c05956.

Cartesian coordinates (TXT)

Structural data, energies for each complex within the DAT20 data set from DFT and CCSD(F12)(T); frontier molecular orbital analysis; natural orbitals for chemical valence; and natural energy decomposition analysis (PDF)

■ AUTHOR INFORMATION

Corresponding Author

Konstantinos D. Vogiatzis − *Department of Chemistry, University of Tennessee, Knoxville, Tennessee 37996, United States;* orcid.org/0000-0002-7439-3850; Email: kvogiatz@utk.edu

https://doi.org/10.1021/acs.jpca.1c05956
J. Phys. Chem. A 2021, 125, 7956−7966

Author

Brett A. Smith − *Department of Chemistry, University of Tennessee, Knoxville, Tennessee 37996, United States;* orcid.org/0000-0003-0258-9704

Complete contact information is available at: https://pubs.acs.org/10.1021/acs.jpca.1c05956

Notes

The authors declare no competing financial interest.

■ ACKNOWLEDGMENTS

The authors gratefully acknowledge the National Science Foundation (CHE-1800237) for financial support of this work and the Advanced Computer Facility (ACF) of the University of Tennessee for computational resources. The authors would like to thank Dr. Jacob Townsend and Gavin Mccarver for their fruitful discussions on the manuscript.

■ REFERENCES

(1) Haaland, A. Covalent versus Dative Bonds to Main Group Metals, a Useful Distinction. *Angew. Chem., Int. Ed.* **1989**, *28*, 992−1007.

(2) Lewis, G. N. *Valence and the Structure of Atoms and Molecules*; The Chemical Catalog Company, Inc., 1923.

(3) Pauling, L. *The Nature of the Chemical Bond and the Structure of Molecules and Crystals*, 3rd ed.; Cornell University: Ithaca, New York, 1938.

(4) Weinhold, F.; Landis, C. R. *A Natural Bond Orbital Donor-Acceptor Perspective*; Cambridge University Press: Cambridge, 2005; pp 89−362.

(5) Plumley, J. A.; Evanseck, J. D. Covalent and Ionic Nature of the Dative Bond and Account of Accurate Ammonia Borane Binding Enthalpies. *J. Phys. Chem. A* **2007**, *111*, 13472−13483.

(6) Lepetit, C.; Maraval, V.; Canac, Y.; Chauvin, R. On the Nature of the Dative Bond: Coordination to Metals and beyond. The Carbon Case. *Coord. Chem. Rev.* **2016**, *308*, 59−75.

(7) Pearson, R. G. Absolute Electronegativity and Hardness: Application to Inorganic Chemistry. *Inorg. Chem.* **1988**, *27*, 734−740.

(8) Jonas, V.; Frenking, G.; Reetz, M. T. Comparative Theoretical Study of Lewis Acid-Base Complexes of BH_3, BF_3, BCl_3, $AlCl_3$, and SO_2. *J. Am. Chem. Soc.* **1994**, *116*, 8741−8753.

(9) Gilbert, T. M. Tests of the MP2 Model and Various DFT Models in Predicting the Structures and B−N Bond Dissociation Energies of Amine−Boranes $(X_3C)_mH_{3-m}B{-}N(CH_3)NH_{3-n}$ (X = H, F; m = 0−3; n = 0−3): Poor Performance of the B3LYP Approach for Dative B−N Bonds. *J. Phys. Chem. A* **2004**, *108*, 2550−2554.

(10) Janesko, B. G. Using Nonempirical Semilocal Density Functionals and Empirical Dispersion Corrections to Model Dative Bonding in Substituted Boranes. *J. Chem. Theory Comput.* **2010**, *6*, 1825−1833.

(11) Frenking, G.; Fröhlich, N. The Nature of the Bonding in Transition-Metal Compounds. *Chem. Rev.* **2000**, *100*, 717−774.

(12) Ruiz, E.; Salahub, D. R.; Vela, A. Density Functional Theory. An Approach to the Quantum Many-Body Problem. *Angew. Chem., lnt. Ed.* **1995**, *117*, 1141−1142.

(13) Ruiz, E.; Salahub, D. R.; Vela, A. Charge-Transfer Complexes: Stringent Tests for Widely Used Density Functionals. *J. Phys. Chem. A* **1996**, *100*, 12265−12276.

(14) Steinmann, S. N.; Piemontesi, C.; Delachat, A.; Corminboeuf, C. Why Are the Interaction Energies of Charge-Transfer Complexes Challenging for DFT? *J. Chem. Theory Comput.* **2012**, *8*, 1629−1640.

(15) Brémond, É.; José Pérez-Jiménez, Á.; Carlos Sancho-García, J.; Adamo, C. Range-Separated Hybrid Density Functionals Made Simple. *J. Chem. Phys.* **2019**, *150*, No. 201102.

(16) Toulouse, J.; Colonna, F.; Savin, A. Long-Range - Short-Range Separation of the Electron-Electron Interaction in Density-Functional Theory. *Phys. Rev. A* **2004**, *70*, No. 062505.

(17) Townsend, J.; Kirkland, J. K.; Vogiatzis, K. D. Post-Hartree-Fock Methods: Configuration Interaction, Many-Body Perturbation Theory, Coupled-Cluster Theory. *Mathematical Physics in Theoretical Chemistry*; Elsevier, 2019; pp 63−117.

(18) Gill, P. M. W.; Head-Gordon, M.; Pople, J. A. An Efficient Algorithm for the Generation of Two-Electron Repulsion Integrals over Gaussian Basis Functions. *Int. J. Quantum Chem.* **1989**, *36*, 269−280.

(19) Helgaker, T.; Klopper, W.; Tew, D. P. Quantitative Quantum Chemistry. *Mol. Phys.* **2008**, *106*, 2107−2143.

(20) Riplinger, C.; Neese, F. An Efficient and near Linear Scaling Pair Natural Orbital Based Local Coupled Cluster Method. *J. Chem. Phys.* **2013**, *138*, No. 034106.

(21) Mitoraj, M.; Michalak, A. Natural Orbitals for Chemical Valence as Descriptors of Chemical Bonding in Transition Metal Complexes. *J. Mol. Model.* **2007**, *13*, 347−355.

(22) Glendening, E. D.; Streitwieser, A. Natural Energy Decomposition Analysis: An Energy Partitioning Procedure for Molecular Interactions with Application to Weak Hydrogen Bonding, Strong Ionic, and Moderate Donor–Acceptor Interactions. *J. Chem. Phys.* **1994**, *100*, 2900−2909.

(23) Glendening, E. D. Natural Energy Decomposition Analysis: Extension to Density Functional Methods and Analysis of Cooperative Effects in Water Clusters. *J. Phys. Chem. A* **2005**, *109*, 11936−11940.

(24) Munárriz, J.; Laplaza, R.; Martín Pendás, A.; Contreras-García, J. A First Step towards Quantum Energy Potentials of Electron Pairs. *Phys. Chem. Chem. Phys.* **2019**, *21*, 4215−4223.

(25) Dapprich, S.; Frenking, G. Investigation of Donor-Acceptor Interactions: A Charge Decomposition Analysis Using Fragment Molecular Orbitals. *J. Phys. Chem. A* **1995**, *99*, 9352−9362.

(26) Mo, Y.; Song, L.; Wu, W.; Zhang, Q. Charge Transfer in the Electron Donor-Acceptor Complex BH_3 NH_3. *J. Am. Chem. Soc.* **2004**, *126*, 3974−3982.

(27) Morokuma, K. Why Do Molecules Interact? The Origin of Electron Donor-Acceptor Complexes, Hydrogen Bonding, and Proton Affinity. *Acc. Chem. Res.* **1977**, *10*, 294−300.

(28) Nandi, A.; Kozuch, S. History and Future of Dative Bonds. *Chem. - Eur. J.* **2020**, *26*, 759−772.

(29) Fisher, L. S.; McNeil, K.; Butzen, J.; Holme, T. A. Theoretical Study of the Role of Boron-Nitrogen Dative Bonds in the Physiological Action of Boronated Compounds. *J. Phys. Chem. B* **2000**, *104*, 3744−3751.

(30) Townsend, J.; Braunscheidel, N. M.; Vogiatzis, K. D. Understanding the Nature of Weak Interactions between Functionalized Boranes and N_2/O_2, Promising Functional Groups for Gas Separations. *J. Phys. Chem. A* **2019**, *123*, 3315−3325.

(31) Mebs, S.; Grabowsky, S.; Förster, D.; Kickbusch, R.; Hartl, M.; Daemen, L. L.; Morgenroth, W.; Luger, P.; Paulus, B.; Lentz, D. Charge Transfer via the Dative N-B Bond and Dihydrogen Contacts. Experimental and Theoretical Electron Density Studies of Small Lewis Acid-Base Adducts. *J. Phys. Chem. A* **2010**, *114*, 10185−10196.

(32) Smith, E. L.; Sadowsky, D.; Cramer, C. J.; Phillips, J. A. Structure, Bonding, and Energetic Properties of Nitrile-Borane Complexes: RCN-BH_3. *J. Phys. Chem. A* **2011**, *115*, 1955−1963.

(33) Eichkorn, K.; Treutler, O.; Öhm, H.; Häser, M.; Ahlrichs, R. Auxiliary Basis Sets to Approximate Coulomb Potentials. *Chem. Phys. Lett.* **1995**, *242*, 652−660.

(34) Grimme, S.; Ehrlich, S.; Goerigk, L. Effect of the Damping Function in Dispersion Corrected Density Functional Theory. *J. Comput. Chem.* **2011**, *32*, 1456−1465.

(35) Grimme, S.; Antony, J.; Ehrlich, S.; Krieg, H. A Consistent and Accurate Ab Initio Parametrization of Density Functional Dispersion Correction (DFT-D) for the 94 Elements H-Pu. *J. Chem. Phys.* **2010**, *132*, No. 154104.

(36) Furche, F.; Ahlrichs, R.; Hättig, C.; Klopper, W.; Sierka, M.; Weigend, F. Turbomole. *Wiley Interdiscip. Rev.: Comput. Mol. Sci.* **2014**, *4*, 91−100.

(37) Perdew, J. P.; Burke, K.; Ernzerhof, M. Generalized Gradient Approximation Made Simple. *Phys. Rev. Lett.* **1996**, *77*, 3865−3868.

(38) Perdew, J. P. Density-Functional Approximation for the Correlation Energy of the Inhomogeneous Electron Gas. *Phys. Rev. B* **1986**, *34*, No. 7406.

(39) Tao, J.; Perdew, J. P.; Staroverov, V. N.; Scuseria, G. E. Climbing the Density Functional Ladder: Nonempirical Meta−Generalized Gradient Approximation Designed for Molecules and Solids. *Phys. Rev. Lett.* **2003**, *91*, No. 146401.
(40) Perdew, J. P.; Ernzerhof, M.; Burke, K. Rationale for Mixing Exact Exchange with Density Functional Approximations. *J. Chem. Phys.* **1996**, *105*, 9982−9985.
(41) Staroverov, V. N.; Scuseria, G. E.; Tao, J.; Perdew, J. P. Comparative Assessment of a New Nonempirical Density Functional: Molecules and Hydrogen-Bonded Complexes. *J. Chem. Phys.* **2003**, *119*, 12129−12137.
(42) Becke, A. D. Density-Functional Thermochemistry. III. The Role of Exact Exchange. *J. Chem. Phys.* **1993**, *98*, 5648−5652.
(43) Zhao, Y.; Truhlar, D. G. The M06 Suite of Density Functionals for Main Group Thermochemistry, Thermochemical Kinetics, Noncovalent Interactions, Excited States, and Transition Elements: Two New Functionals and Systematic Testing of Four M06-Class Functionals and 12 Other Functionals. *Theor. Chem. Acc.* **2008**, *120*, 215−241.
(44) Grimme, S. Semiempirical Hybrid Density Functional with Perturbative Second-Order Correlation. *J. Chem. Phys.* **2006**, *124*, 034108−034111.
(45) Weigend, F.; Ahlrichs, R. Balanced Basis Sets of Split Valence, Triple Zeta Valence and Quadruple Zeta Valence Quality for H to Rn: Design and Assessment of Accuracy. *Phys. Chem. Chem. Phys.* **2005**, *7*, 3297−3305.
(46) Hellweg, A.; Hättig, C.; Höfener, S.; Klopper, W. Optimized Accurate Auxiliary Basis Sets for RI-MP2 and RI-CC2 Calculations for the Atoms Rb to Rn. *Theor. Chem. Acc.* **2007**, *117*, 587−597.
(47) Weigend, F.; Häser, M.; Patzelt, H.; Ahlrichs, R. RI-MP2: Optimized Auxiliary Basis Sets and Demonstration of Efficiency. *Chem. Phys. Lett.* **1998**, *294*, 143−152.
(48) Treutler, O.; Ahlrichs, R. Efficient Molecular Numerical Integration Schemes. *J. Chem. Phys.* **1995**, *102*, 346−354.
(49) Yanai, T.; Tew, D. P.; Handy, N. C. A New Hybrid Exchange-Correlation Functional Using the Coulomb-Attenuating Method (CAM-B3LYP). *Chem. Phys. Lett.* **2004**, *393*, 51−57.
(50) Chai, J. D.; Head-Gordon, M. Systematic Optimization of Long-Range Corrected Hybrid Density Functionals. *J. Chem. Phys.* **2008**, *128*, No. 084106.
(51) Chai, J. D.; Head-Gordon, M. Long-Range Corrected Hybrid Density Functionals with Damped Atom-Atom Dispersion Corrections. *Phys. Chem. Chem. Phys.* **2008**, *10*, 6615−6620.
(52) Neese, F. The ORCA Program System. *WIREs Comput. Mol. Sci.* **2012**, *2*, 73−78.
(53) Vogiatzis, K. D.; Barnes, E. C.; Klopper, W. Interference-Corrected Explicitly-Correlated Second-Order Perturbation Theory. *Chem. Phys. Lett.* **2011**, *503*, 157−161.
(54) Tew, D. P.; Klopper, W.; Neiss, C.; Hättig, C. Quintuple-ζ Quality Coupled-Cluster Correlation Energies with Triple-ζ Basis Sets. *Phys. Chem. Chem. Phys.* **2007**, *9*, 1921−1930.
(55) Hättig, C.; Tew, D. P.; Köhn, A. Accurate and Efficient Approximations to Explicitly Correlated Coupled-Cluster Singles and Doubles, CCSD-F12. *J. Chem. Phys.* **2010**, *132*, No. 231102.
(56) Klopper, W.; Samson, C. C. M. Explicitly Correlated Second-Order Møller-Plesset Methods with Auxiliary Basis Sets. *J. Chem. Phys.* **2002**, *116*, 6397−6410.
(57) Halkier, A.; Helgaker, T.; Jørgensen, P.; Klopper, W.; Koch, H.; Olsen, J.; Wilson, A. K. Basis-Set Convergence in Correlated Calculations on Ne, N_2, and H_2O. *Chem. Phys. Lett.* **1998**, *286*, 243−252.
(58) Frisch, M. J.; Trucks, G. W.; Schlegel, H. B.; Scuseria, G. E.; Robb, M. A.; Cheeseman, J. R.; Scalmani, G.; Barone, V.; Petersson, G. A.; Nakatsuji, H. et al. *Gaussian 16*.Gaussian, Inc.: Wallingford, CT, 2016.
(59) Glendening, E. D.; Badenhoop, J. K.; Reed, A.; Carpenter, J. E.; Bohmann, C. M.; Morales, C. M.; Karafiloglou, P.; Landis, C. R.; Weinhold, F. *NBO 7.0.8., Theoretical Chemistry Institute*. University of Wisconsin, 2018.
(60) Nandy, A.; Zhu, J.; Janet, J. P.; Duan, C.; Getman, R. B.; Kulik, H. J. Machine Learning Accelerates the Discovery of Design Rules and Exceptions in Stable Metal−Oxo Intermediate Formation. *ACS Catal.* **2019**, *9*, 8243−8255.
(61) Nandy, A.; Duan, C.; Janet, J. P.; Gugler, S.; Kulik, H. J. Strategies and Software for Machine Learning Accelerated Discovery in Transition Metal Chemistry. *Ind. Eng. Chem. Res.* **2018**, *57*, 13973−13986.

https://doi.org/10.1021/acs.jpca.1c05956
J. Phys. Chem. A 2021, 125, 7956−7966